A Measurement Method of Motion Parameters in Aircraft Ground Tests Using Computer Vision

Article *in* Measurement · January 2021

DOI: 10.1016/j.measurement.2021.108985

6 authors, including:

Jiashan Cui
Xidian University
35 PUBLICATIONS **161** CITATIONS

SEE PROFILE

Yunhui Li
Shanghai University
16 PUBLICATIONS **52** CITATIONS

SEE PROFILE

Measurement 174 (2021) 108985

Contents lists available at ScienceDirect

Measurement

journal homepage: www.elsevier.com/locate/measurement

A measurement method of motion parameters in aircraft ground tests using computer vision

Jiashan Cui [a], Yunhui Li [b,*], Ju Huo [c], Ming Yang [c], Yongkun Wang [c], Cong Li [d]

[a] School of Aerospace Science and Technology, Xidian University, Xi'an 710126, China
[b] School of Mechatronic Engineering and Automation, Shanghai University, Shanghai 200444, China
[c] School of Astronautics, Harbin Institute of Technology, Harbin 150010, China
[d] Xi'an Branch of China Academy of Space Technology, Xi'an 710100, China

ARTICLE INFO

Keywords:
Machine vision
Aircraft ground test
Intersected planes
Motion parameters
Muti-coordinate system calibration

ABSTRACT

The purpose of this work is aiming at the problem of high precision and large-scale measurement of motion parameters of aircraft ground test. Based on the traditional vision measurement method of motion parameters, a new measurement method of motion parameters based on intersected planes is discussed. Firstly, the measurement of 3D coordinates of laser spots was performed using the 3 D vision technique combined with plane constraints of curtain wall, the images of laser spot projected on the parallel curtain wall were processed using the centroid method, the calibration of multi-coordinates were unified by the unique coordinate system method, then the pose was solved using the proposed method that the normal vector of the intersect plane fixed on the vehicle is used. Finally, according to the measurement principle, the influence of spot center positioning, camera parameter calibration and target geometric error on the calculation results of aircraft motion parameters is analyzed, and the error propagation model is given. The experimental results show that in the measurement range of 8000 mm × 4000 mm × 4000 mm, the measurement error of attitude parameters is less than 0.14°, and the measurement error of position parameters is less than 2 mm. Compared with binocular stereo vision, the accuracy of attitude angle measurement is improved by 100%. Therefore, the measurement method proposed in this paper can achieve high precision and large-scale measurement of the motion parameters of the test aircraft.

1. Introduction

In the ground test of aircraft, the position and attitude of the test aircraft are the basic parameters in the study of kinematics and dynamics, which can be used to check the guidance and control accuracy of the aircraft and to verify the model. At the same time, it is also an important basis for the identification of test results and the determination of possible accident causes [1,2]. In addition, in the ground test of the aircraft, because the measuring equipment such as star sensor and sun sensor cannot work normally, it is necessary to measure the position, attitude and other parameters of the test aircraft through other ways and transmit them to the test aircraft, so as to realize the simulation of star sensor and sun sensor. For this reason, the research on the measurement method of aircraft ground test motion parameters has become one of the essential contents of aircraft ground test technology research.

At present, there are two main methods to measure the motion parameters of aircraft: internal measurement method and external measurement method [3–5]. The internal measurement method of aircraft motion parameters is to load GPS or inertial measurement unit on the aircraft to measure the position and attitude of the aircraft [6]. For aircraft ground test, it is difficult to receive GPS signal in a relatively closed ground laboratory, while the inertial measurement unit is expensive and complex to operate, and there are problems such as long initialization time and error accumulation over time, and its own reliability is also the item to be examined in aircraft ground test. Therefore, it is not suitable to use the internal measurement method to measure the motion parameters of the test aircraft in the ground test. The external measurement method of aircraft motion parameters is a third-party measurement, which uses external equipment (including electronic theodolite [7], radar [8], Moiré fringe ranging method [9], laser tracker [10], iGPS [11], high-speed camera [12–15], etc.) to measure the aircraft motion parameters. Visual measurement is a non-contact measurement method, which develops rapidly in recent years, and is widely used in various measurement fields [16–19]. Depending on the mode of

* Corresponding author.
E-mail address: liyunhui@shu.edu.cn (Y. Li).

https://doi.org/10.1016/j.measurement.2021.108985
Received 18 September 2020; Received in revised form 27 December 2020; Accepted 2 January 2021
Available online 17 January 2021

operation, vision-based motion parameter measurements can be divided into two categories: cooperative target motion parameter measurements and non-cooperative target motion parameters measurements [20–22]. Zhang et al, presented a pose measurement method coupled initial pose measurement with model-based tracking is put forward for space non-cooperative targets. They only focus on the feasibility of the algorithm, but the accuracy is low [20]. In reference [21], a method of measuring pose by coplanar feature is proposed. The requirement for matching target is not to collinear in the direction perpendicular to the imaging plane, and the pose solution has infinite solutions. Pan et al. used a coplanar feature to measure the pose. There are mismatches or mismatches in matching the target, resulting in large error and poor robustness [22]. Cooperative target motion parameter measurement is to install feature device on the moving target and extract the feature information to obtain the target motion parameters. This kind of method has high precision, fast speed and long measuring distance. While, the measurement of non-cooperative target motion parameters does not need to install any device on the moving target It extracts the characteristics of the moving target itself to obtain the target motion parameters. So, there are many disadvantages in the measurement of non-cooperative target motion parameters, such as large computation, slow speed and low measurement accuracy.

According to the number of cameras used in the measurement process, the vision measurement system can be divided into three categories: monocular vision measurement system, binocular vision measurement system and multi eye vision measurement system. The monocular vision measurement system uses a single camera to measure the target's motion parameters. In the measurement process, the two-dimensional plane information of the moving target in space is obtained according to the image information, while the longitudinal depth information is lost. Therefore, when monocular vision is used to measure the space target's motion parameters, other constraints need to be used [23–25]. In [23], a monocular vision pose measurement method is proposed, and an auxiliary constraint fusion mechanism is proposed to position and measure the pose of the aircraft, but the pose measurement accuracy is poor. The binocular vision measurement system uses two cameras to measure the spatial target motion parameters according to the stereo vision measurement principle. It obtains the spatial three-dimensional coordinates of the same feature point on the moving target through different projection positions on the image plane of the two cameras, and then uses the appropriate solution method to solve the target motion parameters [26,27]. Matching of homonymous image points is the key to binocular vision measurement. The measurement principle of the multi vision measurement system is roughly the same as that of the binocular vision measurement system, which is mainly to increase the number of cameras to meet the corresponding measurement range or measurement accuracy requirements when the measurement field is large or the measured structure is complex [28–30].

Whether the above methods are monocular vision pose measurement or stereo vision pose measurement, they are still limited in practical application in ground test of aircraft. The main reason is that the range of motion of the test vehicle is getting larger and larger, the maneuverability is getting stronger and stronger (the attitude angle changes without any constraints), and the test environment is complex (the test vehicle vibrates violently during the test process, and the local position is random emits hot gas flow and high-temperature flame, which covers the full spectrum, and seriously interferes with the measurement of motion parameters). The measurement index is demanding, which makes the traditional vision measurement system unable to meet the corresponding measurement requirements in terms of measurement accuracy, measurement range and environmental adaptability.

In order to meet the needs of high precision and large-scale measurement of flight aircraft ground test motion parameters, the measurement principle and calculation method of aircraft motion parameters measurement system based on cross feature plane are proposed, which realizes high precision and large-scale measurement of flight aircraft motion parameters. The work arrangement of this paper is as follows: In Section 2, we introduced the scheme design of measurement and calculation method of aircraft motion parameters. The method of multi-coordinate system calibration and data conversion is given in Section 3. Section 4 analyzes the error propagation of the measurement system. The experiment and result analysis are carried out in Section 5. Finally, Section 6 presents the conclusion.

2. Principle of aircraft motion parameter measurement

2.1. Principle of pose measurement

The pose measurement system of the aircraft proposed in this paper is shown in Fig. 1. Two feature planes are designed and constructed, which are connected to the aircraft by the laser disk. The laser beam is uniformly laid out in the same plane, which each pair of installation positions are symmetrical with the disk center. A couple of laser tubes are respectively projected on the left and right curtain walls. Each curtain wall has a spot, and the connection of two spots constitutes a beam. The characteristic plane of the laser disk can be fitted by the laser spot projected by multiple beams on the spot receiving wall, and then the normal vector of the characteristic plane can be calculated. Combined with two laser disks arranged at the intersection, two feature planes composed of multiple light spots can be obtained, and then the normal vectors of the two feature planes of spatial intersection can be calculated by fitting. The position and attitude information of the aircraft body can be obtained by calculating the normal vector of the two feature planes and the value of the space intersection in the world coordinate system, and combining the transformation relationship between the aircraft body coordinate system and the aircraft zero coordinate system.

2.2. World coordinate measurement model of projection spot

The measurement of the world coordinates of the projected light spot is to record the image of the projected light spot by the camera, and to solve the world coordinates of the projected light spot by the camera calibration results and the constraints of the projection plane. It is the basis of the aircraft pose solution. The light spot image coordinate is (u, v), the world coordinate is (X_w, Y_w, Z_w), the internal parameter of the camera is matrix $\boldsymbol{A}$. Coordinate system plane XOY of the spot receiving plane 1(2) coincides with spot receiving plane 1(2), and the z-axis direction meets the right-hand criterion, which is perpendicular to the XOY plane. Set the spot receiving plane 1 coordinate system as the world

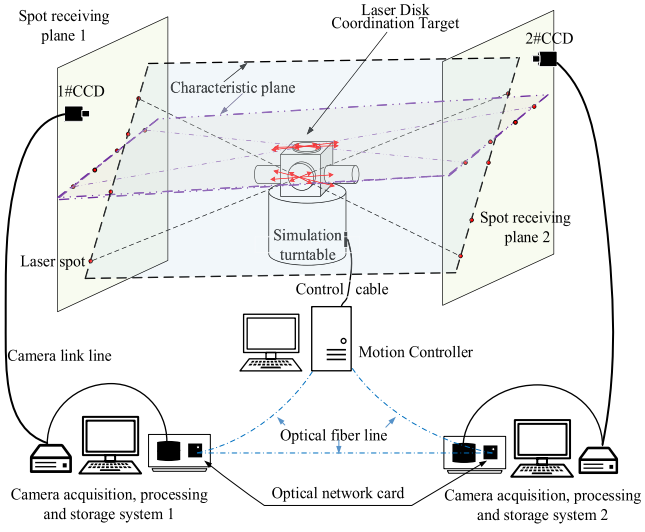

Fig. 1. Aircraft motion parameter measurement overall scheme system diagram.

coordinate system, the conversion relationship between the No.1 camera coordinate system and the spot receiving plane 2 coordinate system is $[R_{c1w2}, T_{w2c1}]$, and the conversion relationship between the No.2 camera coordinate system and the spot receiving plane 1 coordinate system is $[R_{c2w1}, T_{w1c2}]$, then the relationship between the spot image coordinate and the world coordinate can be expressed as:

$$\begin{cases} s\begin{pmatrix} u_j \\ v_j \\ 1 \end{pmatrix} = \boldsymbol{A}_i \begin{bmatrix} \boldsymbol{R}_{ciwk} & \boldsymbol{T}_{wkci} \\ \boldsymbol{0}^T & 1 \end{bmatrix} \begin{pmatrix} X_{wj} \\ Y_{wj} \\ Z_{wj} \\ 1 \end{pmatrix} \\ Z_{wi} = 0 \end{cases} \tag{1}$$

In (1), $i = 1,\cdots,n, j = 1,\cdots,m, k = 1,2$. s is any non-zero factor, i is the number of cameras, the specific layout and number of cameras are shown in Fig. 1, j is the number of spot recorded by the camera, and k is the number of light spot receiving plane.

According to the transformation of coordinate system, the (1) is further simplified as:

$$s\begin{bmatrix} u_j \\ v_j \\ 1 \end{bmatrix} = \boldsymbol{A}_i[\boldsymbol{r}_{1ik} \quad \boldsymbol{r}_{2ik} \quad \boldsymbol{t}_{ik}] \begin{bmatrix} X_{wj} \\ Y_{wj} \\ 1 \end{bmatrix} \tag{2}$$

In (2), $i = 1,\cdots,n, j = 1,\cdots,m, k = 1,2$. $\boldsymbol{r}_1$ and $\boldsymbol{r}_2$ are the 1 and 2 columns of the rotation matrix, and $\boldsymbol{t}$ represents the translation vector.

According to the perspective projection imaging model of the camera, the world coordinates of the light spots 1–4 on light spot receiving plane 1 can be expressed as follows:

$$\begin{cases} X_{wi} = \dfrac{-fr_5T_x + fr_2T_y + Y_ur_8T_x - Y_uT_zr_2 + r_5X_uT_z - T_yX_ur_8}{-X_ur_7r_5 - r_1Y_ur_8 + r_1fr_5 + X_ur_8r_4 + r_2Y_ur_7 - r_2fr_4} \\ Y_{wi} = -\dfrac{-X_ur_7T_y - r_1Y_uT_z + r_1fT_y + X_uT_zr_4 + T_xY_ur_7 - T_xfr_4}{-X_ur_7r_5 - r_1Y_ur_8 + r_1fr_5 + X_ur_8r_4 + r_2Y_ur_7 - r_2fr_4} \\ Z_{wi} = 0 \end{cases} \tag{3}$$

Wherein, $i = 1, 2, 3, 4$, $X_d = s^{-1}dx(u - u_0)$, $Y_d = dy(v - v_0)$, $X_u = X_d\left[1 + k_1\left(X_d^2 + Y_d^2\right)^{1/2}\right]$, $Y_u = Y_d\left[1 + k_1\left(X_d^2 + Y_d^2\right)^{1/2}\right]$. f is the focal length of the camera, d_x and d_y are the horizontal and vertical spacing of the camera sensitive components, (u_0, v_0) is the coordinate of the camera main point in the image coordinate system, $r_1\widetilde{r_8}$ is the rotation matrix element between the camera coordinate system and the spot receiving plane 1 coordinate system (world coordinate system), T_x, T_y, T_z is the translation matrix element between the camera coordinate system and the world coordinate system, which is marked by the camera definitely.

Similarly, under the spot receiving plane 2 coordinate system, the coordinates of spots 5–8 are calculated, and according to the calibration results of the system structure, the world coordinates of spots 5–8 can be obtained as follows:

$$\begin{bmatrix} X_{w1i} \\ Y_{w1i} \\ Z_{w1i} \end{bmatrix} = \boldsymbol{R}_{w1w2}\begin{bmatrix} X_{w2i} \\ Y_{w2i} \\ Z_{w2i} \end{bmatrix} + \boldsymbol{T}_{w2w1}(i = 5, 6, 7, 8) \tag{4}$$

In (4), $\boldsymbol{R}_{w1w2}$ and $\boldsymbol{T}_{w1w2}$ are the rotation and translation relations between spot receiving plane 1 and 2 respectively, and i is the spot number.

2.3. Aircraft pose calculation model

Suppose that there are two feature planes M_1 and M_2 on the target, and the normal vectors of the feature planes are L_1 and L_2 respectively. The direction vectors of L_1 and L_2 in the aircraft body coordinate system and the world coordinate system are $\boldsymbol{L_{w1}}$, $\boldsymbol{L_{w2}}$ and $\boldsymbol{L_{m1}}$, $\boldsymbol{L_{m2}}$ separately, and the coordinates of the spatial intersection N are X_m and X_w. The normal vector of the feature planes and its intersection is shown in Fig. 2:

The transformation relationship between world coordinate system

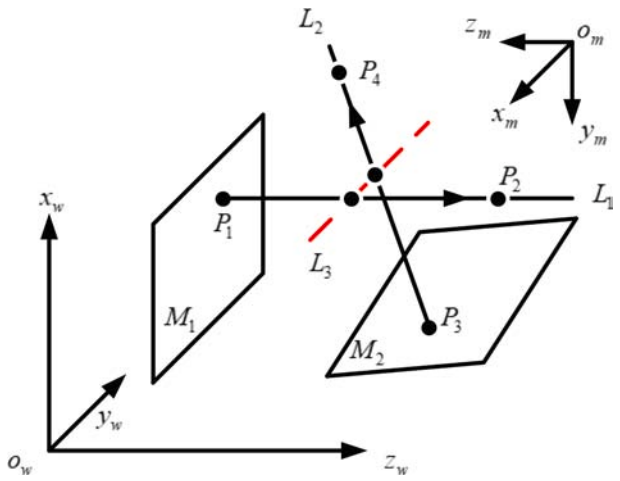

Fig. 2. The characteristic planes normal vector and its intersection point.

$O_wx_wy_wz_w$ and aircraft body coordinate system $O_mx_my_mz_m$ is defined as:

$$O_wx_wy_wz_w = R_{wm}O_mx_my_mz_m + T_{mwo} \tag{5}$$

Let P_1 and P_2 be two non-coincident points of normal vector L_1, and P_3 and P_4 be the two non-coincident points of normal vector L_2. L_3 is the perpendicular of L_1 and L_2. At a certain time, the values of two coordinate systems corresponding to each point meet the following relationship:

$$P_{wi} = R_{wm}P_{mi} + T_{mwo}(i = 1, 2, 3, 4) \tag{6}$$

Where, P_{wi} is the value of P_i $(i = 1, 2, 3, 4)$ in the world coordinate system. P_{mi} is the value of P_i in the aircraft body coordinate system. R_{wm} is the inverse matrix of the rotation matrix R_{mw} of the aircraft body coordinate system $O_mx_my_mz_m$ relative to the world coordinate system $O_wx_wy_wz_w$. T_{mwo} is the position vector of the origin of the aircraft body coordinate system $O_mx_my_mz_m$ in the world coordinate system $O_wx_wy_wz_w$.

Then the normal vectors of the two feature planes can be expressed in the world coordinate system as follows:

$$\begin{cases} \boldsymbol{L_{w1}} \triangleq \dfrac{P_{w2} - P_{w1}}{|P_{w2} - P_{w1}|} \\ \boldsymbol{L_{w2}} \triangleq \dfrac{P_{w4} - P_{w3}}{|P_{w4} - P_{w3}|} \end{cases} \tag{7}$$

Similarly, the normal vector of the feature plane is expressed in the aircraft body coordinate system as follows:

$$\begin{cases} \boldsymbol{L_{m1}} \triangleq \dfrac{P_{m2} - P_{m1}}{|P_{m2} - P_{m1}|} \\ \boldsymbol{L_{m2}} \triangleq \dfrac{P_{m4} - P_{m3}}{|P_{m4} - P_{m3}|} \end{cases} \tag{8}$$

Combining (6) can obtain:

$$\begin{cases} \boldsymbol{L_{w1}} = R_{wm}\boldsymbol{L_{m1}} \\ \boldsymbol{L_{w2}} = R_{wm}\boldsymbol{L_{m2}} \end{cases} \tag{9}$$

In the same way, we can get the relationship between vectors $\boldsymbol{L_{w1}}$ and $\boldsymbol{L_{w2}}$ as follows:

$$\begin{aligned} \boldsymbol{L_{w1}} \times \boldsymbol{L_{w2}} &= (R_{wm}\boldsymbol{L_{m1}}) \times (R_{wm}\boldsymbol{L_{m2}}) \\ &= R_{wm}(\boldsymbol{L_{m1}} \times \boldsymbol{L_{m2}}) \end{aligned} \tag{10}$$

Because the two feature planes intersect, the normal vectors of the two feature planes are not parallel, so we can know that both sides of (10) are non-zero vectors, and find the normalized unit vector, and we can get:

$$\frac{\boldsymbol{L_{w1}}\times\boldsymbol{L_{w2}}}{|\boldsymbol{L_{w1}}\times\boldsymbol{L_{w2}}|}=R_{wm}\frac{\boldsymbol{L_{m1}}\times\boldsymbol{L_{m2}}}{|\boldsymbol{L_{m1}}\times\boldsymbol{L_{m2}}|} \tag{11}$$

Definitions $\boldsymbol{B_w}$ and $\boldsymbol{B_m}$ are:

$$\begin{cases}\boldsymbol{B_w}=\dfrac{\boldsymbol{L_{w1}}\times\boldsymbol{L_{w2}}}{|\boldsymbol{L_{w1}}\times\boldsymbol{L_{w2}}|}\\ \boldsymbol{B_m}=\dfrac{\boldsymbol{L_{m1}}\times\boldsymbol{L_{m2}}}{|\boldsymbol{L_{m1}}\times\boldsymbol{L_{m2}}|}\end{cases} \tag{12}$$

Then (12) can be expressed as:

$$\boldsymbol{B_w}=R_{wm}\boldsymbol{B_m} \tag{13}$$

Definitions $\boldsymbol{D_w}$ and $\boldsymbol{D_m}$ are:

$$\begin{cases}\boldsymbol{D_w}\equiv[\boldsymbol{L_{w1}}\quad\boldsymbol{L_{w2}}\quad\boldsymbol{B_w}]\\ \boldsymbol{D_m}\equiv[\boldsymbol{L_{m1}}\quad\boldsymbol{L_{m2}}\quad\boldsymbol{B_m}]\end{cases} \tag{14}$$

Combining (9), (13) and (14), it can be concluded that:

$$\boldsymbol{D_w}=R_{wm}\boldsymbol{D_m} \tag{15}$$

It can be seen from the intersection of two characteristic planes that $\boldsymbol{D_w}$ and $\boldsymbol{D_m}$ are full rank matrices with inverse matrices. The following equation can be deduced from (15):

$$R_{mw}=R_{wm}^{-1}=\left(\boldsymbol{D_w}\boldsymbol{D_m}^{-1}\right)^{-1} \tag{16}$$

According to the above definition, because the aircraft to be tested is a rigid body and two feature planes are fixed on the aircraft to be tested, then the spatial intersection point N (the midpoint of the common vertical line) of the normal vectors of the two feature planes can be defined as the feature points fixed to the aircraft body. Then the position vector of the conversion relationship between the aircraft body coordinate system and the world coordinate system can be obtained by the following equation:

$$T_{mwo}=\boldsymbol{X_w}-R_{wm}\boldsymbol{X_m} \tag{17}$$

At this point, the measurement method of aircraft body motion parameters based on the normal vector of intersecting feature planes is deduced. As long as the value of the normal vector of the intersecting feature planes of aircraft body in the aircraft body coordinate system and the world coordinate system and the intersection coordinate of the two normal vectors can be obtained, the position and attitude of aircraft body can be calculated.

In practical application, the measurement of aircraft motion parameters needs to obtain its pose parameters relative to the initial zero position of aircraft body at any time. It is necessary to establish the conversion relationship between aircraft body coordinate system and aircraft body zero position coordinate system (i.e. T_{wm_0o}, R_{m_0w}), which will be described in detail in the subsequent calibration process.

2.4. Solution model of aircraft motion parameter measurement

According to the motion parameter measurement principle derived above, the solution of the problem of aircraft pose measurement is transformed into the process of determining the values of two vectors L_1 and L_2 in the world coordinate system and the aircraft coordinate system at different times and the intersection of the two vectors.

As shown in Fig. 2, in order to construct the above vectors L_1 and L_2 on the aircraft, two identical laser disks are designed in this paper, which are composed of a series of laser transmitters installed in the same plane and at the center of symmetry of the disk center. When two laser discs are installed on the aircraft, the projection spot of the laser emitted by them on the left and right curtain walls will form two characteristic planes. Through the plane fitting process, we can get the normal vectors of two characteristic planes on the aircraft. According to the above calculation, the pose parameters of the aircraft can be obtained from two normal vectors.

2.5. Characteristic plane and its normal vector

As shown in Fig. 3, the four beams emitted by the laser disk leave four laser spots on the left and right curtain walls M_1 and M_2 respectively, P_1, P_2, P_3, P_4 on the left curtain wall and P_5, P_6, P_7, P_8 on the right curtain wall. In this paper, eight characteristic spot are used to simulate the characteristic plane of the laser disk.

The coordinate of the laser spot in the world coordinate system $O_wx_wy_wz_w$ is $\{P_i=(x_i,y_i,z_i), i=1,2,\cdots,n\}$ (in the actual experiment, if four pairs of laser beams are used, then $n=8$). In addition, if the coordinates of each spot on the fitting plane M_A is $\{P_i^*=(x_i+v_{x_i},y_i+v_{y_i},z_i+v_{z_i}), i=1,2,\cdots,n\}$ respectively, then the error of each spot in the x, y and z direction can also be considered as $\{E_i^*=(v_{x_i},v_{y_i},v_{z_i}), i=1,2,\cdots,n\}$, so the spatial plane equation is:

$$z_i+v_{zi}=a(x_i+v_{xi})+b(y_i+v_{yi})+c \tag{18}$$

a, b and c are the plane parameter to be calculated, and the (18) is sorted into matrix expression as follows:

$$(\boldsymbol{A}+\boldsymbol{E_A})\boldsymbol{X}=\boldsymbol{Y}+\boldsymbol{E_Y} \tag{19}$$

Where $\boldsymbol{E_A}$ is the error matrix of matrix $\boldsymbol{A}$, $\boldsymbol{A}=\begin{bmatrix}x_1 & y_1 & 1\\ \vdots & \vdots & \vdots\\ x_i & y_i & 1\end{bmatrix}$ and $\boldsymbol{E_Y}$ is the error vector of vector $\boldsymbol{Y}$, $\boldsymbol{Y}=[z_1\ \cdots\ z_i]^T$, $\boldsymbol{X}=[a\quad b\quad c]^T$.

In this paper, SVD method is used to solve (19), and the least square solution is obtained as follows:

$$[\boldsymbol{A}\quad\boldsymbol{L}]=\begin{bmatrix}\underset{m+1}{\boldsymbol{U_1}} & \underset{n-(m+1)}{\boldsymbol{U_2}}\end{bmatrix}\begin{bmatrix}\boldsymbol{\Sigma}\\ 0\end{bmatrix}\boldsymbol{V^T}=\boldsymbol{U_1}\boldsymbol{\Sigma}\boldsymbol{V^T} \tag{20}$$

Wherein:

$$\boldsymbol{V^T}=\begin{bmatrix}V_{11} & V_{12}\\ V_{21} & V_{22}\end{bmatrix}\begin{matrix}m\\ 1\end{matrix},\ \boldsymbol{U_1}=\begin{bmatrix}U_{11} & U_{12}\\ m & 1\end{bmatrix},\ \boldsymbol{\Sigma}=\begin{bmatrix}\Sigma_1 & 0\\ 0 & \Sigma_2\\ m & 1\end{bmatrix}\begin{matrix}m\\ 1\end{matrix} \tag{21}$$

Then the least square solution of the plane parameter is:

$$\boldsymbol{X_{TLS}}=-\boldsymbol{V_{12}}\boldsymbol{V_{22}^{-1}} \tag{22}$$

It can also be expressed as:

$$\boldsymbol{X_{TLS}}=\left(\boldsymbol{A^TA}-\sigma_3^2\boldsymbol{I}\right)^{-1}\boldsymbol{A^TL} \tag{23}$$

Which, σ_3 is the minimum eigenvalue of $[\boldsymbol{A}\quad\boldsymbol{L}]$.

Through the calculation of the above formula, the parameter solution of the fitting plane can be obtained, and the normal vector of plane M_A in the world coordinate system $O_wx_wy_wz_w$ can be expressed as:

$$\boldsymbol{L_A}=(a\quad b\quad -1) \tag{24}$$

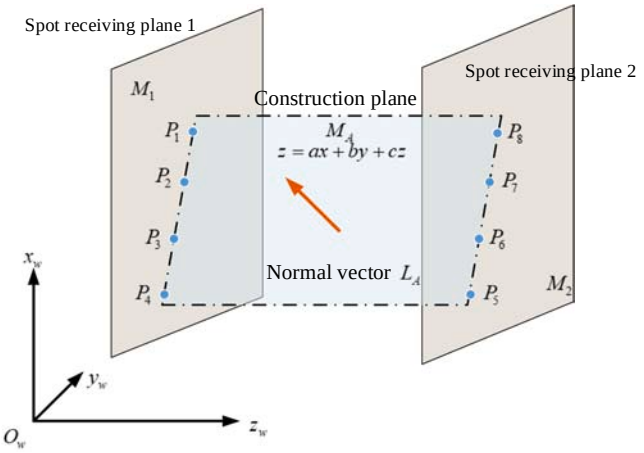

Fig. 3. Sketch map of characteristic plane fitting in world coordinate system.

Similarly, two laser planes can be fitted and their normal vectors can be calculated.

2.6. Calculation method of laser disk center position

The value of the normal vector of the fitting plane in the world coordinate system $O_w x_w y_w z_w$ is calculated in the Section 3. *A*. However, in order to get the intersection point of the two normal vectors in space, it is necessary to get the position origin N_A of the normal vector of the fitting plane. It can be seen from Fig. 4 that four beams L_1, L_2, L_3, L_4 have six intersections in space, and the intersection of two beams is defined as $N_{ij} = \begin{pmatrix} x_{ij} & y_{ij} & z_{ij} \end{pmatrix} \quad (i,j = 1,2,\cdots,n \ \ i \neq j)$. In this paper, the origin of the normal vector L_1 in the fitting plane is defined as the average value of all beam space intersections, that is:

$$N_A\begin{pmatrix} x_A & y_A & z_A \end{pmatrix} = \frac{1}{C_n^2}\sum_{i=1}^{n}\begin{pmatrix} x_{ij} & y_{ij} & z_{ij} \end{pmatrix} \tag{25}$$

Wherein, C_n^2 is combination (taking 2 non repetitive elements from n different elements to form a subset), $i,j = 1,2,\cdots,n$ and $i \neq j$.

Considering that there are six intersection points of four beams in space, a point is fitted as the center of the laser disk. In this paper, the coordinate value of each spatial intersection is given the weight λ, which is defined as:

$$\lambda_{ij} = 1/\left(d_{ij}\right) \quad (i,j = 1,2,\cdots,n \ \ i \neq j, d_{ij} \neq 0) \tag{26}$$

Where, d_{ij} is the distance between lines on different planes in space, and the setting weight is inversely proportional to the distance between lines on different surfaces. When two lines in space are in the same plane and the distance value is 0, the weight of this point is 1. Therefore, the coordinates of the center point of the laser disk with weight can be calculated as:

$$N_A\begin{pmatrix} x_A & y_A & z_A \end{pmatrix} = \frac{\sum_{i=1}^{n}\lambda_{ij}\begin{pmatrix} x_{ij} & y_{ij} & z_{ij} \end{pmatrix}}{\sum \lambda_{ij}} \tag{27}$$

Wherein, $(i,j = 1,2,\cdots,n)$ and $i \neq j$.

According to the same method, the center position of the first excited disk can be obtained, and then the position of the aircraft can be obtained according to the intersection algorithm of the straight lines of different planes in space. The algorithm of pose parameters measurement based on intersected plane can be described as follows:

Step 1: Install two circular laser discs on the aircraft, and project their spot to the spot receiving walls on both sides;

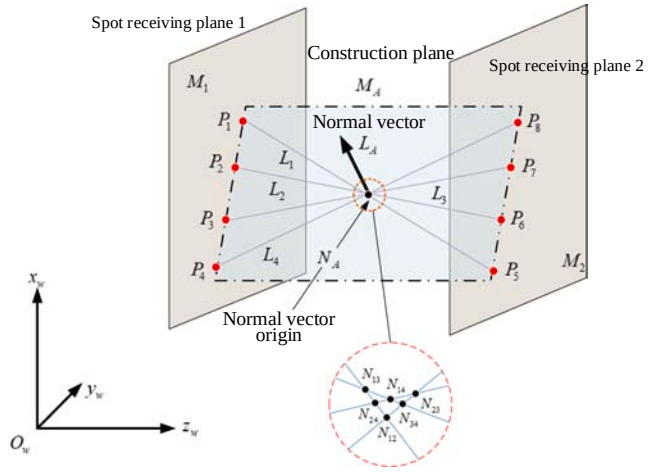

Fig. 4. Schematic diagram of characteristic plane center point in world coordinate system.

Step 2: Imaging the spot with the camera, get the three-dimensional coordinates of the spot in the world coordinate system by solving the wall constraint, and then get two vectors L_1 and L_2 fixed on the aircraft by plane fitting;

Step 3: According to the attitude solution algorithm of Section 2. *C*, the attitude parameter $\boldsymbol{R}_{mw}$ of the aircraft can be calculated;

Step 4: Calculate the center of each laser disk according to the symmetrical arrangement feature of the beam on the laser disk, and estimate the rotation center $\boldsymbol{T}_0$ of the aircraft from the center of two laser disks;

Step 5: Combined with the position of Section 2. *C* and the intermediate algorithm, the position parameter T_{mw0} of the aircraft can be obtained.

In the actual test, two problems need to be solved:

(1) The three-dimensional coordinates of the spot on the curtain wall are solved by camera imaging;
(2) The unification of multi-coordinate system and the transformation of related data in measurement system.

In order to get the three-dimensional coordinates of the spot, it is necessary to calibrate the camera. We arrange some black points on the spot receiving plane as the calibration points (as shown in Fig. 15). It constructs a large and small plane calibration board together with the curtain wall, and obtains the three-dimensional coordinate value of the calibration points through the total station measurement. Then through the parameter calibration between the camera coordinate system and the curtain wall coordinate system, the necessary parameters are provided for the subsequent solution of the three-dimensional coordinates of the spot on the curtain wall through camera imaging and curtain wall constraint. See reference [30] for the specific process of camera calibration.

3. Multi-coordinate system calibration and data conversion method

3.1. Calibration of multi-coordinate system

The coordinate system which involved in the visual measurement motion parameters of the aircraft ground test mainly includes the aircraft body coordinate system, the ground coordinate system and the two spot receiving plane coordinate systems. One spot receiving plane coordinate system is selected as the world coordinate system, and the aircraft body coordinate system and the ground coordinate system coincide at the initial time.

In this paper, the spot receiving plane coordinate system $O_{p1} x_{p1} y_{p1} z_{p1}$

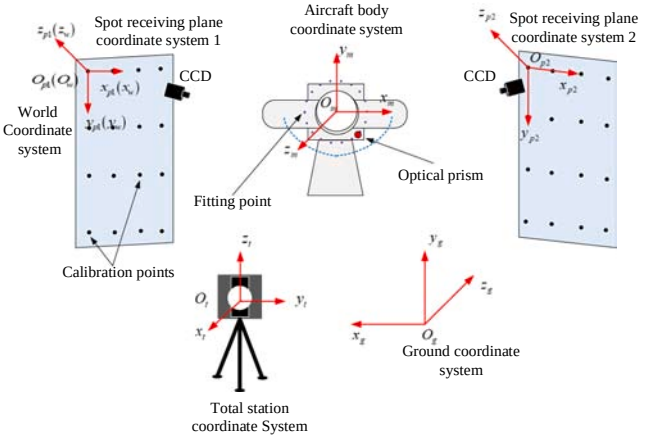

Fig. 5. Schematic diagram of coordinate systems during aircraft ground test.

may be selected as the world coordinate system $O_w x_w y_w z_w$, and each coordinate system in the measurement system is shown in Fig. 5.

In the measurement process, according to the image coordinates and camera model parameters of the cooperative target beam projection spot, the three-dimensional coordinates of the projection spot in the corresponding spot receiving plane coordinate system can be obtained. In order to obtain the three-dimensional coordinates of the projected light spot in the world coordinate system. It is necessary to establish the conversion relationship between the spot receiving plane coordinate system and the world coordinate system. At the same time, according to the measurement principle of the motion parameters based on the beam vector, the motion parameters of the test aircraft in the world coordinate system can be obtained directly. In order to obtain the motion parameters of the test aircraft in the ground coordinate system, it is necessary to establish the conversion relationship between the world coordinate system and the ground coordinate system. The establishment of coordinate system transformation relationship is also called coordinate system calibration.

In this paper, the calibration of multi-coordinate system in the visual measurement system of aircraft ground test motion parameters is realized by total station. In the calibration process, the receiving plane coordinate system of spot and the aircraft body coordinate system at the initial time is established through the total station measurement data. Then, taking the total station coordinate system as the intermediate coordinate system, the conversion relationship between the receiving plane coordinate system of spot and the world coordinate system and between the world coordinate system and the ground coordinate system is obtained.

3.2. Data conversion in multi-coordinate system

In the measurement process, according to the principle of motion parameter measurement based on the beam vector, the rotation matrix $\boldsymbol{R}_{mw}$ from the world coordinate system to the aircraft body coordinate system and the position vector $\boldsymbol{T}_{mwo}$ of the origin of the aircraft body coordinate system in the world coordinate system can be measured directly. In order to obtain the rotation matrix $\boldsymbol{R}_{mg}$ from the ground coordinate system to the aircraft body coordinate system and the position vector $\boldsymbol{T}_{mgo}$ of the origin of the aircraft body coordinate system in the ground coordinate system, the following transformations can be performed:

$$\begin{cases} \boldsymbol{R}_{mg} = \boldsymbol{R}_{mw}\boldsymbol{R}_{wg} = \boldsymbol{R}_{mw}\boldsymbol{R}_{gw}^{-1} \\ \boldsymbol{T}_{mgo} = \boldsymbol{R}_{gw}\boldsymbol{T}_{mwo} + \boldsymbol{T}_{wgo} \end{cases} \tag{34}$$

Wherein, $\boldsymbol{R}_{gw}$ is the rotation matrix from the world coordinate system to the ground coordinate system, and $\boldsymbol{T}_{wgo}$ is the position vector of the origin of the world coordinate system in the ground coordinate system. $\boldsymbol{R}_{gw}$, $\boldsymbol{T}_{wgo}$ can be found in Section 4. *B*.

In the whole measurement process, the data conversion relationship between coordinate systems of the measurement system is shown in Fig. 6.

As shown in Fig. 7, this paper constructs the world coordinate system and the aircraft body coordinate system with the help of the calibration device, and establishes the relationship between them. Through the calibration device, the scanning points on the curtain walls of the left and right are used to fit the spot receiving plane, and the plane coordinate system (*i.e.* the world coordinate system) of the spot receiving is constructed, so as to establish the relationship between the coordinate system of the calibration device and the plane coordinate system of the spot receiving; then the calibration device cooperates with the prism to calibrate the flight simulator and fit the coordinate system of the aircraft simulation device (i.e. the aircraft body coordinate system). The relationship between the calibration device and the aircraft simulation device coordinate system is established. Finally, the relationship between the house coordinate system (the world coordinate system) and the aircraft simulation device coordinate system (the aircraft body coordinate system) is established.

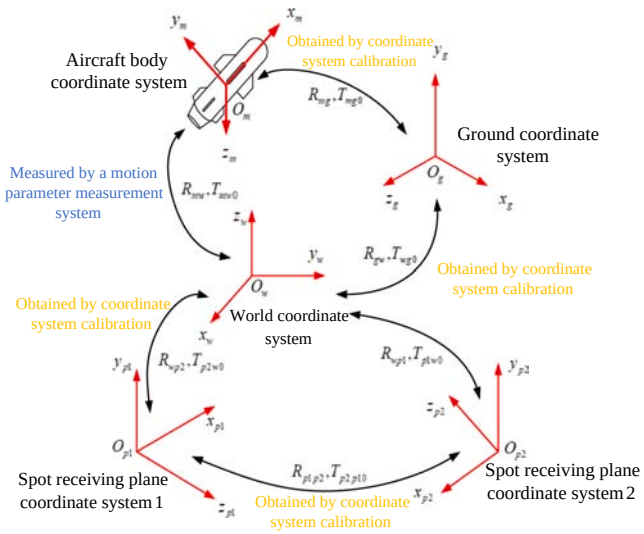

Fig.6. Diagram of transformation relationship among coordinate systems.

4. Error analysis of pose measurement

Based on the principle of pose measurement in this paper, it is essentially based on the change of cross beam mapping on the image, and then the pose change parameters of the target can be obtained by a certain functional relationship. According to the theory of error propagation, because there are errors in the image points, the function will inevitably contain errors. The parameters of the feature points in the image plane are the direct measurement and the pose parameters is the indirect measurement. In order to analyze the pose parameters measurement accuracy, the error transfer relationship of this paper is analyzed. The measurement errors in this paper are mainly summarized as: spot center positioning error, camera external parameter calibration error and beam straightness error.

4.1. Analysis of spot center positioning error

According to the projected spot world coordinate measurement model, combined with the error theory, it can be known that the three-dimensional coordinate measurement error of the characteristic light spot can be expressed as:

$$\begin{cases} \partial x_{wi} = \dfrac{\partial x_{wi}}{\partial u_i}\delta u_i + \dfrac{\partial x_{wi}}{\partial v_i}\delta v_i \\ \partial y_{wi} = \dfrac{\partial y_{wi}}{\partial u_i}\delta u_i + \dfrac{\partial y_{wi}}{\partial v_i}\delta v_i \end{cases} \quad (i = 1, \cdots 8) \tag{35}$$

Where, δu_i and δv_i are the image coordinate extraction errors, i is the feature point on the spot receiving plane, and j is the spot receiving plane. Therefore, the error transfer model between the images coordinates of feature points and the three-dimensional coordinates can be obtained from (35) as follows:

$$\delta \boldsymbol{W} = \boldsymbol{E}_{wP}\delta \boldsymbol{P} \tag{36}$$

Wherein, $\delta \boldsymbol{W} = \left(\partial x_{w1}, \cdots, \partial x_{w8}, \partial y_{w1}, \cdots, \partial y_{w8}\right)^{\mathrm{T}}$ is the world coordinate measurement error vector. $\delta \boldsymbol{P} = (\delta u_1, \cdots, \delta u_8, \delta v_1, \cdots, \delta v_8)^{\mathrm{T}}$ is the image coordinate error vector.

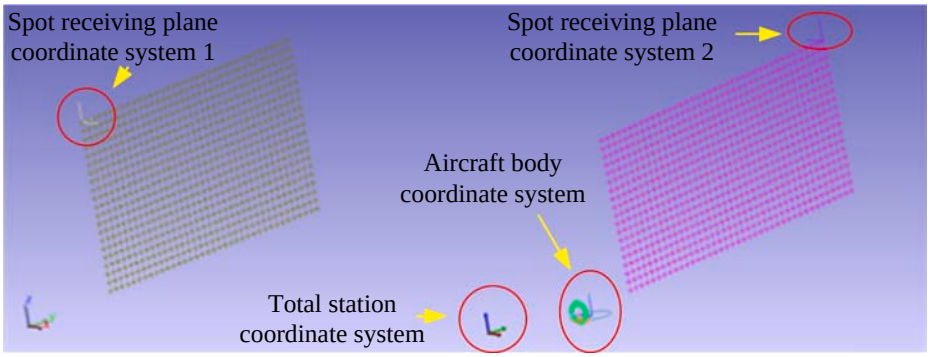

Fig. 7. Panorama fitting of coordinate systems. Each coordinate system relation in the measurement process.

$$E_{wP}=\begin{bmatrix} \frac{\partial x_{w1}}{\partial u_1} & 0 & \cdots & \frac{\partial x_{w1}}{\partial v_1} & 0 & \cdots \\ 0 & \frac{\partial x_{w2}}{\partial u_2} & \cdots & 0 & \frac{\partial x_{w2}}{\partial v_2} & \cdots \\ \vdots & \vdots & \cdots & \vdots & \vdots & \cdots \\ \frac{\partial y_{w1}}{\partial u_1} & 0 & \cdots & \frac{\partial y_{w1}}{\partial v_1} & 0 & \cdots \\ 0 & \frac{\partial y_{w2}}{\partial u_2} & \cdots & 0 & \frac{\partial y_{w2}}{\partial v_2} & \cdots \\ \vdots & \vdots & \cdots & \vdots & \vdots & \cdots \end{bmatrix}_{16\times 16}$$ is the error transfer model between image coordinates and world coordinates.

4.2. Analysis of camera parameter calibration error

Camera calibration is divided into internal parameter calibration and external parameter calibration. The internal parameters mainly include focal length f, radial distortion coefficient k_1, etc.. The external parameters mainly include camera and world coordinate rotation matrix $\boldsymbol{R}(\theta_x,\theta_y,\theta_z)$ and translation vector $\boldsymbol{T}(t_x,t_y,t_z)$. Because the internal parameters can be pre-calibrated with high-precision calibration equipment in advance, this paper mainly analyzes the error of the camera external parameters calibration to the three-dimensional coordinate measurement of the spot, which can be expressed as follows:

$$\begin{cases} \partial x_{wi}=\frac{\partial x_{wi}}{\partial \theta_x}\delta\theta_x+\frac{\partial x_{wi}}{\partial \theta_y}\delta\theta_y+\frac{\partial x_{wi}}{\partial \theta_z}\delta\theta_z+\frac{\partial x_{wi}}{\partial t_x}\delta t_x+\frac{\partial x_{wi}}{\partial t_y}\delta t_y+\frac{\partial x_{wi}}{\partial t_z}\delta t_z \\ \partial y_{wi}=\frac{\partial y_{wi}}{\partial \theta_x}\delta\theta_x+\frac{\partial y_{wi}}{\partial \theta_y}\delta\theta_y+\frac{\partial y_{wi}}{\partial \theta_z}\delta\theta_z+\frac{\partial y_{wi}}{\partial t_x}\delta t_x+\frac{\partial y_{wi}}{\partial t_y}\delta t_y+\frac{\partial y_{wi}}{\partial t_z}\delta t_z \end{cases} \tag{37}$$

Therefore, the error transfer model for the three-dimensional coordinates of the feature points can be obtained from the external camera calibration according to (37):

$$\delta \boldsymbol{W}=\boldsymbol{E}_{wA}\delta \boldsymbol{A} \tag{38}$$

Wherein, $\delta \boldsymbol{W}=\left(\partial x_{w1},\cdots,\partial x_{w8},\partial y_{w1},\cdots,\partial y_{w8}\right)^{\mathrm{T}}$ is the world coordinate measurement error vector. $\delta \boldsymbol{A}=\left(\delta\theta_x,\delta\theta_y,\delta\theta_z,\delta t_x,\delta t_y,\delta t_z\right)^{\mathrm{T}}$ is the calibration error vector of camera external parameters. $\boldsymbol{E}_{wA}=\begin{bmatrix} \frac{\partial x_{w1}}{\partial \theta_x} & \frac{\partial x_{w1}}{\partial \theta_y} & \cdots & \frac{\partial x_{w1}}{\partial t_z} \\ \vdots & \vdots & \ddots & \vdots \\ \frac{\partial y_{w8}}{\partial \theta_x} & \frac{\partial y_{w8}}{\partial \theta_y} & \cdots & \frac{\partial y_{w8}}{\partial t_z} \end{bmatrix}_{16\times 6}$ is the calibration error vector of camera external parameters.

4.3. Analysis of cooperative target geometric error

As shown in Fig. 8, ideally, the target laser beam projected onto the two spot receiving planes should be collinear and coplanar. However, due to the manufacturing error of the target, the beams may not be collinear and may not be coplanar. Thus, we divide the matching target error into horizontal straightness error $\varepsilon_{-\mathrm{hor}}$ and vertical straightness error $\varepsilon_{-\mathrm{ver}}$.

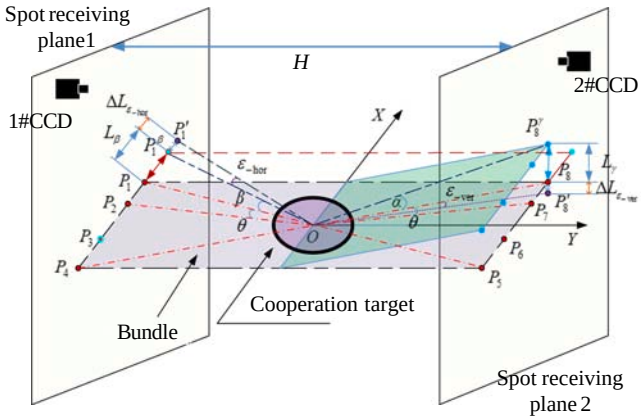

Fig. 8. Geometric error description diagram of cooperative target.

We use the angle between the ideal beam and the actual beam to represent the horizontal straightness error $\varepsilon_{-\mathrm{hor}}$. For the convenience of analysis, we assume that when the aircraft is performing yaw motion, ideally P_1 moves to P_1^{β} along the X-direction. Due to the existence of errors caused by the horizontal straightness of the target, P_1 actually moves to $P_1^{'}$. Then, the error $\Delta L_{\varepsilon_{-\mathrm{hor}}}$ caused by the horizontal straightness of the target is:

$$\Delta L_{\varepsilon_{-hor}}=\frac{H}{2}\left[tan(\theta+\beta+\varepsilon_{-hor})-tan(\beta+\varepsilon_{-hor})\right] \tag{39}$$

Where, H is the distance between the two spot receiving planes, θ is the angle between the target laser beams, β is the yaw motion angle of the aircraft, and $\varepsilon_{-\mathrm{hor}}$ is the horizontal straightness of the cooperative target. Therefore, the error propagation model of the horizontal straightness and the three-dimensional coordinate measurement error of the beam projection characteristic point is expressed as:

$$\begin{bmatrix} x_w \\ y_w \end{bmatrix}=\begin{bmatrix} \Delta L_{\varepsilon_{-\mathrm{hor}}} \\ 0 \end{bmatrix}+\begin{bmatrix} x_w^{'} \\ y_w^{'} \end{bmatrix} \tag{40}$$

For the vertical straightness, all beams of the cooperative target are in the same plane π under ideal condition. Due to the existence of processing errors, all beams are not coplanar. For the convenience of analysis, we use the angle between the beam and the ideal plane π to represent the vertical straightness error $\varepsilon_{-\mathrm{ver}}$. As shown in Fig. 8, it is assumed that P_8 moves along the Y-direction to P_8^{γ} ideally when the aircraft is rolling. In fact, $P_8^{'}$ moves to P_8^{γ} due to the error caused by the horizontal straightness of the target. Then, the error $\Delta L_{\varepsilon_{-\mathrm{ver}}}$ caused by the vertical straightness of the target is:

$$\Delta L_{\varepsilon_{-\mathrm{ver}}} = \frac{H\tan(\varepsilon_{-\mathrm{ver}} + \arctan(\cos\theta + \tan\gamma))}{2\cos\theta} \tag{41}$$

Where, H is the distance between the two spot receiving planes, θ is the angle between the target laser beams, γ is the roll motion angle of the aircraft, and $\varepsilon_{-\mathrm{ver}}$ is the vertical straightness of the cooperative target. Therefore, the error propagation model of the vertical straightness and the three-dimensional coordinate measurement error of the beam projection characteristic point is expressed as:

$$\begin{bmatrix} x_w \\ y_w \end{bmatrix} = \begin{bmatrix} 0 \\ \Delta L_{\varepsilon_{-\mathrm{ver}}} \end{bmatrix} + \begin{bmatrix} x_w^{'} \\ y_w \end{bmatrix} \tag{42}$$

Based on the above, the error propagation relationship between the geometric error of cooperative target and the three-dimensional coordinates of the spot is expressed as follows:

$$\delta \boldsymbol{W} = \boldsymbol{E}_{wG}\delta \boldsymbol{G} \tag{43}$$

Wherein, $\delta \boldsymbol{W} = \left(\partial x_{w1}, \cdots, \partial x_{w8}, \partial y_{w1}, \cdots, \partial y_{w8}\right)^{\mathrm{T}}$ is the world coordinate measurement error vector. $\delta \boldsymbol{G} = \left(\partial x_{w1}^{'}, \cdots, \partial x_{w8}^{'}, \partial y_{w1}^{'}, \cdots, \partial y_{w8}^{'}\right)^{\mathrm{T}}$ is the geometric error vector of the cooperative target processing. $\boldsymbol{E}_{wG} = \begin{bmatrix} 1+\Delta L_{\varepsilon_{-\mathrm{hor}}} & 0 & 0 & 0 & \cdots & 0 \\ 0 & \ddots & 0 & 0 & \cdots & 0 \\ \vdots & \vdots & 1+\Delta L_{\varepsilon_{-\mathrm{hor}}} & \vdots & \vdots & \vdots \\ 0 & 0 & 0 & 1+\Delta L_{\varepsilon_{-\mathrm{ver}}} & \cdots & 0 \\ \vdots & \vdots & \vdots & \vdots & \ddots & \vdots \\ 0 & 0 & 0 & 0 & 0 & 1+\Delta L_{\varepsilon_{-\mathrm{ver}}} \end{bmatrix}_{16\times 16}$ is the geometric error propagation model of the cooperative target.

4.4. Error propagation model between three-dimensional coordinate of spot and pose measurement

If the ideal rotation transformation matrix is $\boldsymbol{R}_{wm}$ between the target coordinate system and the measurement coordinate system, and the spot coordinate P_i, $i = 1, 2, \cdots, n$ are known, according to the pose solution model, the error transfer function of the three-dimensional coordinate measurement error $\delta \boldsymbol{W}$ to the position solution is:

$$\delta \boldsymbol{T}_{mwo} = \delta X_w - \boldsymbol{R}_{wm}\delta X_m \tag{44}$$

Where, X_w is the midpoint of the vertical line of the beams in the world coordinate system, X_m is the midpoint of the vertical line of the beams in the target coordinate system, and $\boldsymbol{R}_{wm}$ is the rotational transformation relationship between the target coordinate system and the measurement coordinate system.

And because

$$\boldsymbol{R}_{mw} = \left(\boldsymbol{D}_w \cdot \boldsymbol{D}_m^{-1}\right)^{-1} \tag{45}$$

From the complete differential property of matrix, we can get:

$$\delta \boldsymbol{R}_{wm} = \delta \boldsymbol{D}_w \boldsymbol{D}_m^{-1} + \boldsymbol{D}_w \delta\left(\boldsymbol{D}_m^{-1}\right) \tag{46}$$

Wherein, $\boldsymbol{D}_m = (\boldsymbol{A}_{m1}, \boldsymbol{A}_{m2}, \boldsymbol{B}_m)$, $\boldsymbol{D}_w = (\boldsymbol{A}_{w1}, \boldsymbol{A}_{w2}, \boldsymbol{B}_w)$, $\delta \boldsymbol{D}_w = (\delta \boldsymbol{A}_{w1}, \delta \boldsymbol{A}_{w2}, \delta \boldsymbol{B}_w)$, $\delta \boldsymbol{D}_m = (\delta \boldsymbol{A}_{m1}, \delta \boldsymbol{A}_{m2}, \delta \boldsymbol{B}_m)$.

Among them, $\delta \boldsymbol{B}_w = \frac{\delta \boldsymbol{A}_{w1} \times \delta \boldsymbol{A}_{w2}}{|\delta \boldsymbol{A}_{w1} \times \delta \boldsymbol{A}_{w2}|}$, $\delta \boldsymbol{B}_m = \frac{\delta \boldsymbol{A}_{m1} \times \delta \boldsymbol{A}_{m2}}{|\delta \boldsymbol{A}_{m1} \times \delta \boldsymbol{A}_{m2}|}$, $\delta \boldsymbol{A}_{wj} = \frac{\delta P_{w(j+2)} - \delta P_{wj}}{\left|P_{w(j+2)} - P_{wj}\right|}$, $\delta \boldsymbol{A}_{mj} = \frac{\delta P_{m(j+2)} - \delta P_{mj}}{\left|P_{m(j+2)} - P_{mj}\right|}$, $j = 1, 2$, $\delta P_{wi} = (\delta X_{wi}, \delta Y_{wi}, \delta Z_{wi})$, $i = 1, \cdots, 8$.

Therefore

$$\begin{aligned} \delta \boldsymbol{R}_{mw} &= \delta\left(\boldsymbol{R}_{wm}\right)^{-1} = -\left(\delta \boldsymbol{R}_{wm}\right)^{-2} \\ &= -\left(\delta \boldsymbol{R}_{wm}^{-1} \delta \boldsymbol{R}_{wm}^{-T}\right) \end{aligned} \tag{47}$$

(44) and (45) can be further expressed as:

$$\delta\left[\boldsymbol{T}_{mw0}, \boldsymbol{R}_{mw}\right]^{\mathrm{T}} = \delta f\left(P_{wi}\right)(i = 1, \cdots 8) \tag{48}$$

Wherein, $\boldsymbol{T}_{mw0}$ and $\boldsymbol{R}_{mw}$ are aircraft body postures, and P_{wi} is the three-dimensional world coordinate of the beam projection feature points. Then, we will get

$$\delta \boldsymbol{q} = \left(\boldsymbol{J}_f^T \boldsymbol{J}_f\right)^{-1} \boldsymbol{J}_f^T \delta \boldsymbol{Q} \tag{49}$$

In which, $\boldsymbol{J}_f$ is the Jacobian matrix, $\delta \boldsymbol{q}$ is the pose measurement error of the aircraft, and $\delta \boldsymbol{Q}$ is the three-dimensional coordinate measurement error of the spot.

Let $\boldsymbol{E}_P = \left(\boldsymbol{J}_f^T \boldsymbol{J}_f\right)^{-1} \boldsymbol{J}_f^T$, then the error propagation model between three-dimensional coordinate measurement and pose solution can be expressed as:

$$\delta \boldsymbol{q} = \boldsymbol{E}_P \delta \boldsymbol{Q} \tag{50}$$

According to the above error analysis, we will get the global error propagation mode between the pose calculation error and the image coordinate extraction error, camera external parameter calibration error, and the geometric error of the cooperative target can be expressed as:

$$\delta \boldsymbol{A} = \boldsymbol{E}_p \boldsymbol{E}_{wP} \boldsymbol{E}_{wA} \boldsymbol{E}_{wG} \delta \boldsymbol{P} \tag{51}$$

Wherein, $\delta \boldsymbol{A} = (\delta T_{mw0}, \delta R_{mw})^T$, and $\delta \boldsymbol{P}$ is the three-dimensional coordinate measurement error of the spot.

Without considering the coupling relationship among image error, camera external parameter calibration error and beam straightness, the error propagation matrix of aircraft body pose measurement system based on laser projection feature points can be obtained as follows:

$$\boldsymbol{E}_I = \boldsymbol{E}_P(\boldsymbol{E}_{wP} + \boldsymbol{E}_{wA} + \boldsymbol{E}_{wG}) \tag{52}$$

5. Experiment and result analysis

In order to achieve the practicability of the aircraft's motion parameter measurement algorithm proposed in this paper, and accuracy of the error propagation function, which is verified by simulation experiment and actual experiment.

5.1. Simulation experiment and result analysis

In the simulation experiment, the distance between the spot receiving plane is set to $L = 11{,}000$ mm, the transformation relationship between the two spot receiving plane coordinate systems is $R_{12}(0^\circ, 0^\circ, 0^\circ)$ and $T_{12} = (8000, 0, 0)$, and the angle between the cooperative target beams is set to $\theta = 15^\circ$.

Assuming that the origin of the aircraft coordinate system is the intersection point $O = (4000, 4000, 1800)$ of the cooperative target beam, the axis of the aircraft coordinate system is defined to coincide with the angular bisector of the two lines, and the rotation around Z-axis is defined as the pitch angle α, and the rotation around Y-axis is defined as the yaw angle β, The rotation around X-axis is defined as the roll angle γ, and the relationship between the world coordinate system and the reference launcher is $R_{1m0}(0^\circ, 0^\circ, 0^\circ)$ and $T_{1m0} = (4000, 4000, 1800)$. The specific settings of the camera parameters are shown in Table 1. Among them, the ideal image coordinates of the laser projection spot are calculated by perspective projection model.

In order to verify the effectiveness of the proposed method, the three-

Table 1
The camera parameter set in simulation experiment.

Camera	Cam_1	Cam_2
Internal parameters	$\begin{bmatrix} 200 & 0 & 1280 \\ 0 & 200 & 1024 \\ 0 & 0 & 1 \end{bmatrix}$	$\begin{bmatrix} 200 & 0 & 1280 \\ 0 & 200 & 1024 \\ 0 & 0 & 1 \end{bmatrix}$
External parameters	$\boldsymbol{R} = \boldsymbol{0}$ $\boldsymbol{T}$=[4000 4000 4000]	$\boldsymbol{R} = \boldsymbol{0}$ $\boldsymbol{T}$=[4000 4000 4000]
f/mm	27	27
k_1	3×10^{-3}	3×10^{-3}

dimensional coordinate positioning error is assumed to be 2 mm, and $(\alpha, \beta, \gamma) = (10sin(0.2\pi t), 20cos(0.2\pi t), 0.5t)$. The traditional stereo vision direct linear solution method (TM) and the algorithm proposed in this paper (PM) are respectively used to measure the aircraft motion parameters, and the maximum error of the two methods are shown in Table 2.

From Table 2, we can get that the accuracy of the pose parameters calculation method PM is much higher than TM, which is mainly because the method proposed in this paper enlarges the baseline of pose parameters measurement compared to TM. The difference between the two methods in the position calculation error is not large, mainly because the method proposed in this paper has a large range of beam projection space, and the absolute coordinates of the spot world coordinates differ greatly, which leads to the calculation instability of the coordinate value of the intersection point of the two beams. The position of the intersection point is prone to large deviations. On the other hand, according to the position calculation principle, it is known that the position calculation error in the direction of the *Y*-axis is related to the pitch angle calculation error, which is why the pitch angle error is greater than the yaw and roll angle. So, in general, the accuracy of the PM is higher than TM.

In order to analyze the error propagation accuracy of the method proposed in this paper, the aircraft motion is set as $(\alpha, \beta, \gamma) = (10sin(0.2\pi t), 20cos(0.2\pi t), 10cos(0.2\pi t))$. The extraction error of laser projection characteristic spot image coordinates obeys the influence of Gaussian distribution noise with mean value of 0 and variance of [0,1] *pixe*l. The rotation angle error level of camera external parameters is set to mean value of 0, variance of [0, 0.1]°, and the mean value of translation vector error is 0 and variance of [0,10] mm. The specific setting of ideal camera parameters is shown in Table 1. The vertical straightness and horizontal straightness mean value of the beam is 0, and the variance is [0, 0.1]°. Monte Carlo method is used for simulation, and the results are shown in Fig. 9, Fig. 10 and Fig. 11.

It can be seen from Fig. 9 (a) and (b) that the error of attitude measurement increases with the increase of position error of spot positioning error, among which the error of pitch angle is larger than that of the other two, mainly because the baseline of pitch angle measurement is shorter than the other two axes, and the error of position measurement is basically proportional to extraction error of spot image coordinates, in which the error of *Z*-axis direction is much larger than that of other axes.

From Fig. 10 (a) and (b), it can be seen that the measurement results of beam straightness to position increase with the increase of the angle of motion. The straightness of the beam has little influence on the attitude measurement results, which can be ignored in some applications, but has great influence on the position measurement results. This is mainly related to the principle of solving the intersection of the beam, which is affected by the straightness error, resulting in the intersection of the beams to produces a large error affects the position measurement result.

As shown in Fig. 11 (a) and (b), the camera external parameter calibration has a great influence on the position and attitude measurement results, especially on the pitch angle accuracy. It is worth noting that the influence on the *X* and *Y* axes is much larger than that on the *Y*-axis in Fig. 11 (b). This is because the distance between the two spot receiving plane is far larger than the camera field of view.

5.2. Actual experiment and result analysis

In this paper, in the process of visual measurement and test of aircraft ground test motion parameters, firstly, the calibration of the measurement system is completed according to the multi-coordinate system calibration method in Section 4. The total station used in the calibration process is Sokkia NET 0.5AX, which positioning accuracy is 0.5 mm. In this experiment, based on the rotation angle of each axis given by the attitude setting device, the spatial pose parameters of the aircraft body calculated by the system are tested when the three axes are moving separately and in three-axis simultaneous-motioned. In order to facilitate the accuracy comparison of experimental parameters, the pose parameters calculated by the system are converted to the coordinate system at the zero moment of the motion of the attitude given device, then the measured angle is the angle value of the corresponding axis rotation of the attitude given device, because the space position of the attitude given device is constant, the theoretical value of the space position obtained by the solution should be 0.

In the experiment, and the unit is degree. The exercise time of a single experiment was 10 s. In the experiment, the pitch axis motion track is set as $\alpha = 10sin(0.2\pi t)$, the yaw axis motion track is set as $\beta = 20cos(0.2\pi t)$, and the roll axis motion track is set as $\gamma = 0.5t$.

In the experiment, the image resolution of the two cameras is 1280 × 1024, the frame rate of image acquisition is 100 Hz, the exposure time of image acquisition is 5 *ms*, and the camera acquisition clock is triggered synchronously by the attitude setting device. The experimental site is 8000 mm × 4000 mm × 4000 mm, and the wall size of one side curtain wall is 4000 mm × 4000 mm, the measurement distance is about 8000 mm, the FOV on the wall is about 4000 × 4000 mm^2 on the wall, the measurement accuracy of the laser spot is about 2 mm. In each cooperative target, The laser beam is uniformly laid out in the same plane, as shown in Fig. 12. The angle setting error of attitude setting device is less than 20″. Other relevant parameters of the measurement system are shown in Table 3

5.3. Analysis of three-axis independent motion test results

The following shows the space pose parameters of the aircraft calculated by the system when the three-axis is moving alone, as shown in Fig. 13. It can be seen from the figure that there is no coupling when the three-axis moves alone, and the calculated attitude angle is within 0.1° and the position error is within 1.5 mm.

It can be seen from Fig. 13 that in the test, when only the pitch angle moves, the angle measurement error is less than 0.1°, and the pitch angle measurement error is greater than the roll angle and yaw angle measurement error. This is mainly because the measurement experiment, the pitch angle measurement baseline is relatively short, which makes the pitch angle measurement accuracy more affected by the beam projection spot positioning noise. Accordingly, only when the pitch angle moves, the *Z*-direction position measurement error is larger than the *X*-direction and *Y*-direction position measurement error.

5.4. Analysis of the test results of three-axis simultaneous-motioned

In the three-axis simultaneous-motioned, the output information of the motion track of the attitude given device in the experiment, and the data of the space attitude angle and displacement calculated by the aircraft parameter solution system are shown in Table 4, where α', β' and γ' represent the data of the pitch angle, roll angle and yaw angle of the aircraft (attitude given device) motion calculated by the aircraft motion parameter solution system respectively, and T_x, T_y, T_z represent the calculated data respectively. The displacement of aircraft motion relative to the zero time aircraft coordinate system.

From the Table 4, it can be seen that the average value of the PM for position calculation is not much different, but the RMSE (Root Mean Square Error) is small, which shows that the result of position calculation in this paper is stable. For the attitude calculation results, the average value and RMSE of PM method are smaller than that of TM.

Table 2
Comparison of measurement results of pose measurement methods.

Method	*α/°*	*β/°*	*γ/°*	*x/mm*	*y/mm*	*z/mm*
TM	0.321	0.262	0.272	1.615	1.833	1.677
PM	0.112	0.133	0.072	1.653	2.095	1.756

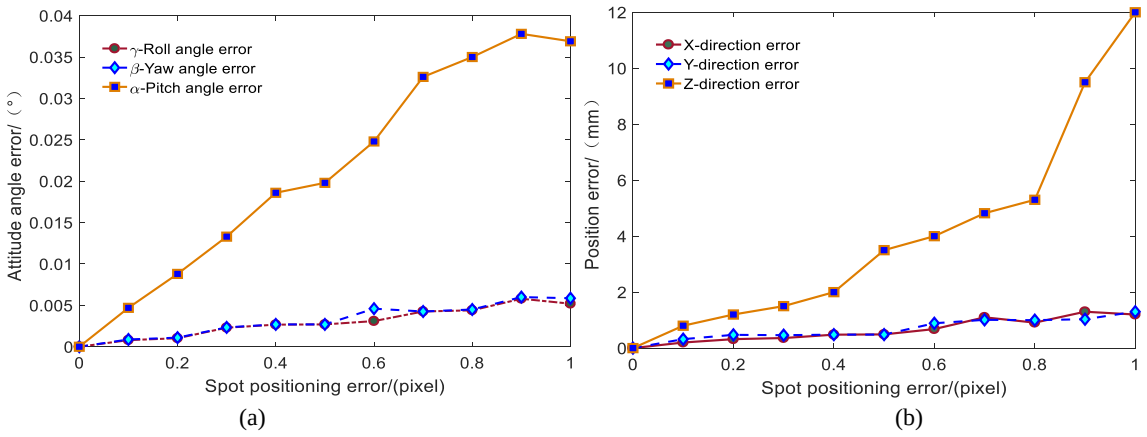

Fig. 9. Relationship between pose measurement error and spot image coordinate positioning error. (a) Attitude angle error. (b) Position error.

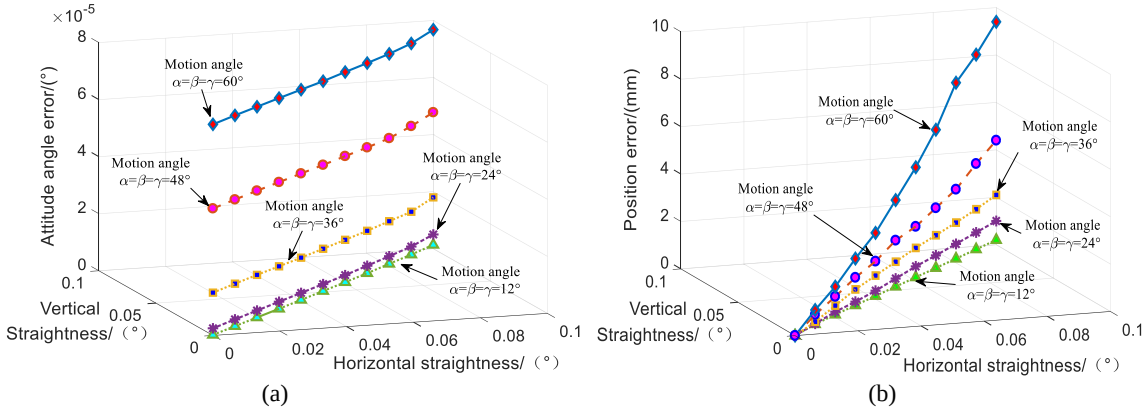

Fig. 10. Relationship between pose measurement error and geometric error of cooperative target. (a) Attitude angle error. (b) Position error.

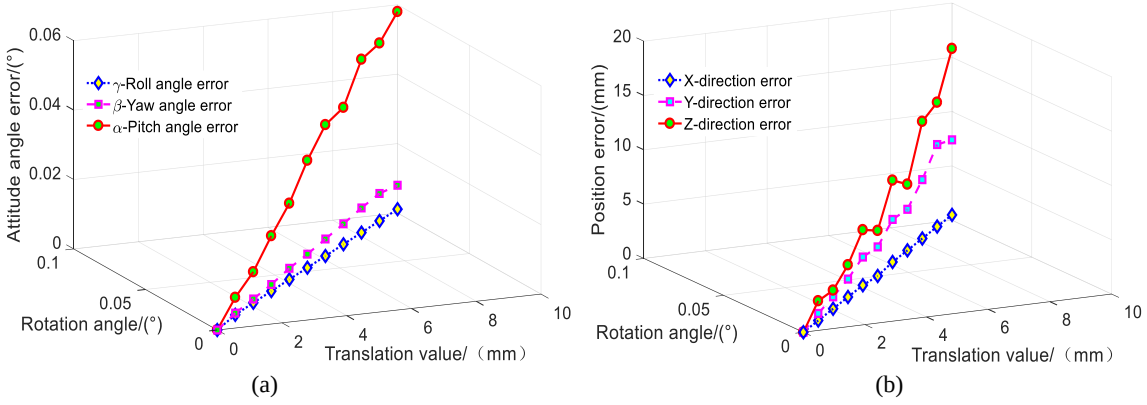

Fig. 11. Relationship between pose measurement error and camera external parameter calibration error. (a) Attitude angle error. (b) Position error.

Generally speaking, PM method is better than TM method in stability. In terms of calculation accuracy, the position calculation accuracy is similar, but the attitude calculation accuracy is high.

The calculated curves of attitude angle α', β' and γ' and position T_X, T_Y, T_Z (the position input value is 0) are shown in Fig. 14, and the errors distribution are shown in Fig. 15.

In the experiment of three-axis simultaneous-motioned, the measurement errors of pitch angle, roll angle and yaw angle are larger than that of three-axis individual motion test results, which are caused by the coupling error of three-axis simultaneous-motioned pose solution. The above analysis is also applicable to the error analysis of position measurement in *X*-direction, *Y*-direction and *Z*-direction. From the whole point of view, the accuracy error of attitude measurement is less 0.14° and the position measurement error is less 2 mm by using cross laser and measuring target. The experimental results demonstrate that the design method in this paper can achieve high precision and large scale measurement of the motion parameters of the test aircraft.

6. Conclusion

In order to meet the needs of the external measurement system of aircraft space motion parameters, the measurement principle and

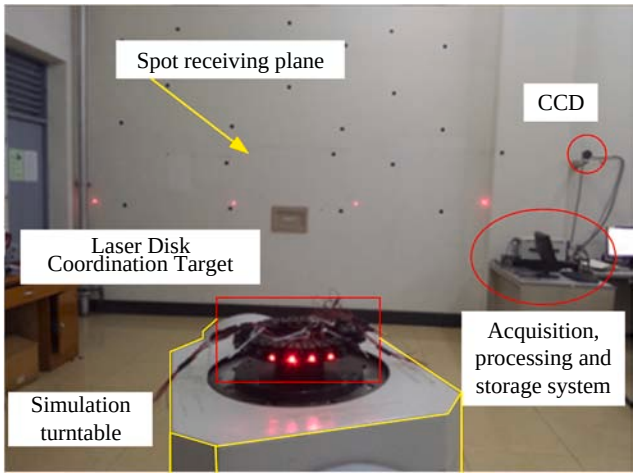

Fig. 12. Hardware-in-the-loop simulation device for test aircraft. Experimental environment.

Table 3
Test parameters.

Index	parameters
System parameters	$R_{mw} = \begin{bmatrix} -1.0000 & 0.0002 & -0.0046 \\ 0.0002 & 1.0000 & 0.0004 \\ 0.0046 & 0.0004 & -1.0000 \end{bmatrix}$ $T_{mw} = [2629.5586 \quad 2902.3159 \quad 4903.8978]$
Calibration error	1.2 mm
Image spot error extraction error	0.2pixel
Straightness of cooperative target	1′
Coordinate system calibration error	0.5 mm

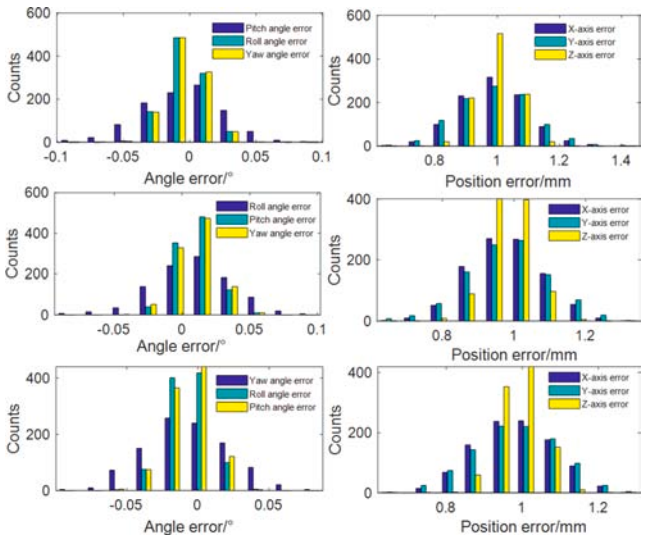

Fig. 13. Measurement results of motion parameters in three-axis independent motion experiment.

calculation method of the measurement system of aircraft motion parameters based on the cross feature plane is designed. Firstly, the two intersecting feature planes are connected with the measured aircraft, and the calculation method of the aircraft's space pose are obtained by using the characteristic that the normal vector of the plane intersects in space and the relative position remains unchanged. In this measurement

Table 4
Part of the experimental data of the motion track in three-axis simultaneous-motioned.

Index	$\alpha(°)$	$\beta(°)$	$\gamma(°)$	PM			TM			PM			TM		
Frame				$\alpha'(°)$	$\beta'(°)$	$\gamma'(°)$	$\alpha'(°)$	$\beta'(°)$	$\gamma'(°)$	T_x(mm)	T_y(mm)	T_z(mm)	T_x(mm)	T_y(mm)	T_z(mm)
0	0.000	20.000	0.000	0.000	20.000	0.000	0.000	20.000	0.000	0.278	1.236	0.678	0.197	0.538	0.704
100	5.877	16.180	0.500	5.965	16.312	0.587	6.315	16.412	0.617	0.19	0.859	0.685	0.569	1.038	0.850
200	9.51	6.180	1.000	9.595	6.511	1.112	9.695	6.611	1.218	0.621	0.724	0.965	0.206	0.514	1.078
300	9.51	−6.180	1.500	9.595	−6.356	1.627	9.895	−6.88	1.322	0.278	1.176	0.862	0.242	1.573	0.597
400	5.877	−16.180	2.000	5.965	−16.207	2.049	6.265	−15.547	2.247	0.132	1.331	0.774	0.355	1.096	0.778
500	0.000	−20.000	2.500	0.085	−19.768	2.585	0.575	−19.168	2.715	0.586	1.467	0.952	0.219	1.255	1.170
600	−5.877	−16.180	3.000	−5.791	−16.148	3.037	−5.591	−16.348	3.237	0.358	1.373	0.781	0.659	1.176	0.786
700	−9.510	−6.180	3.500	−9.422	−6.127	3.535	−9.322	−6.447	3.729	0.575	1.447	0.784	0.378	0.904	1.153
800	−9.510	6.180	4.00	−9.424	6.211	4.057	−9.624	6.685	4.271	0.645	1.180	0.780	0.703	1.091	1.083
900	−5.877	16.180	4.500	−5.791	16.311	4.536	−5.791	16.511	4.372	0.571	1.401	0.876	0.309	1.277	1.170
1000	0.000	20.000	5.000	0.025	20.032	5.058	0.190	20.532	5.183	0.555	1.352	0.778	0.736	0.964	1.150
Average error				0.072	0.070	0.062	0.164	0.144	0.066	0.435	1.231	0.810	0.415	1.038	0.956
Std. deviation				0.058	0.420	0.099	0.591	1.419	0.483	0.601	0.760	0.298	0.667	0.982	0.681
RMSE				0.030	0.134	0.037	0.193	0.389	0.167	0.190	0.240	0.094	0.210	0.310	0.215

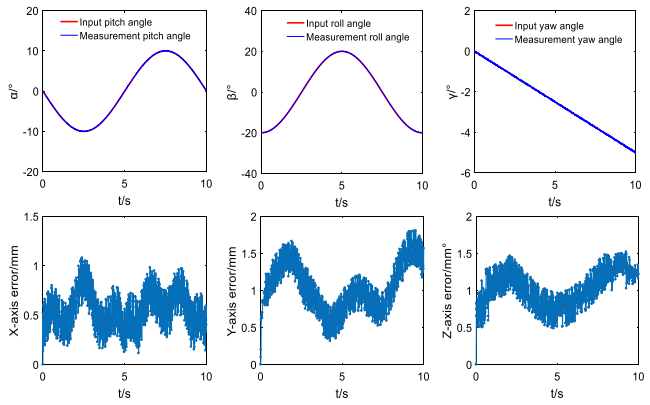

Fig. 14. Schematic diagram of experimental output value and calculated value.

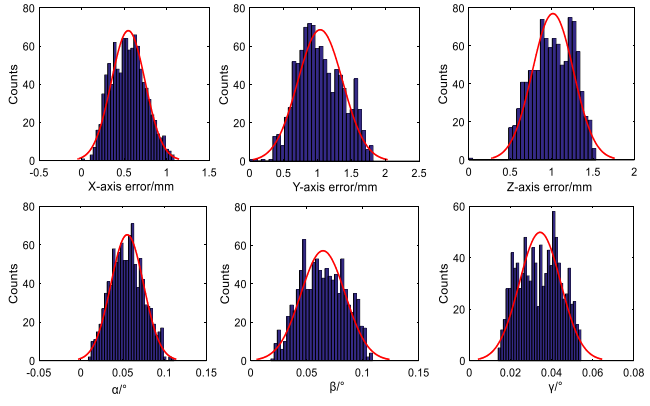

Fig. 15. Histogram of measurement error distribution of motion parameters.

method, the Characteristic plane is constructed based on the fitting of the feature points on the plane, and its normal vector is obtained. Then the position and attitude of the aircraft in space can be obtained according to the calculated method. Then, the coordinate system involved in the measurement of aircraft ground test motion parameters is analyzed, and the corresponding coordinate system calibration and data conversion methods are given. Finally, the visual measurement performance of the aircraft ground test motion parameters is tested by simulation and experiment. The test results show that the visual measurement method can meet the measurement requirements of attitude parameter measurement error less than 0.14° (3σ) and position parameter measurement error less than 2 mm (3σ) under the condition of 8000 mm × 4000 mm × 4000 mm of space, and can achieve high-precision and large-scale measurement of the test aircraft's motion parameters.

The measurement method of motion parameters based on the cross feature plane transforms the measurement of the fixed feature points on the test vehicle into the measurement of any light points on the straight beam, which breaks through the restriction of the geometric conditions of the test vehicle, increases the measurement baseline and improves the measurement accuracy of the motion parameters. On this basis, the measurement range and accuracy of ground vehicle motion parameters can be improved by increasing the number of linear beams in cooperative target, and the singularity of transformation from rotation matrix to Euler angle caused by large-scale fast motion can also be solved.

CRediT authorship contribution statement

Jiashan Cui: Conceptualization, Methodology, Visualization, Writing - original draft. **Yunhui Li:** Software, Formal analysis, Writing - review & editing. **Ju Huo:** Formal analysis. **Ming Yang:** . **Yongkun Wang:** Conceptualization, Formal analysis. **Cong Li:** .

Declaration of Competing Interest

The authors declare that they have no known competing financial interests or personal relationships that could have appeared to influence the work reported in this paper.

Acknowledgments

This work was supported by the China Postdoctoral Science Foundation under Grant 2019M653870XB, National Natural Science Foundation of Shanxi Province under Grant no.2020GY-003, 2020JQ-292, National Science Fund of China under Grants 61603034, 62001340 and Fundamental Research Funds for the Central Universities, China, XJS191315, JC2007.

References

[1] M. Bulman, Ground Testing of a Nuclear Thermal Rocket, in: Proc. 47th AIAA/ASME/SAE/ASEE Joint Propul. Conf. & Exhibit, Aug. 2011, AIAA 2011-5849.
[2] M. S. Brown, G. C. Herring, K. Cabell, et al., Optical measurements at the combuster exit of the HIFiRE2 ground test engine, in: Proc. 50th AIAA Aerosp. Sci. Meeting including the New Horizons Forum and Aerosp. Exposition, Jan. 2012, AIAA 2012-0857.
[3] C.E. Cohen, B.W. Parkinson, B.D. McNally, Flight tests of attitude determination using GPS compared against an inertial navigation unit, J. Navigat. 41 (1) (1994) 83–97.
[4] S.C. Lee, S.K. Hong, Velocity-aided attitude estimation for helicopter aircraft using microelectromechanical system inertial-measurement units, Sensors 16 (12) (2016) 2102.
[5] F.F. Chen, D.J. Kang, J.H. Park, New measurement method of Poisson's ratio of PVA hydrogels using an optical flow analysis for a digital imaging system, Meas. Sci. Technol. 24 (5) (2013), 055602.
[6] J. Luo, Z. Wang, Z. Wen, M. Li, S. Liu, C. Shen, Reflector automatic acquisition and pointing based on auto-collimation theodolite, Rev. Sci. Instrum. 89 (1) (2018), 015101.
[7] D.H. Shin, D.H. Jung, D.C. Kim, J.W. Ham, S.O. Park, A distributed FMCW radar system based on fiber-optic links for small drone detection, IEEE Trans. Instrum. Meas. 66 (2) (2017) 340–347.
[8] K.S. Yen, M.M. Ratnam, Simultaneous measurement of 3-D displacement components from circular grating moire fringes: an experimental approach, Opt. Laser. Eng. 50 (6) (2012) 887–899.
[9] G. Zhang, C.Y. Zhang, X.S. Jing, Z.L. Sun, Y.X. Zhang, M. Luo, Station-transfer measurement accuracy improvement of laser tracker based on photogrammetry, Measurement 94 (2016) 717–725.
[10] Q. Zeng, X. Huang, S.G. Li, Z.P. Deng, High-efficiency posture prealignment method for large component assembly via iGPS and laser ranging, IEEE Trans. Instrum. Meas. 69 (8) (2020) 5497–5510.
[11] Z. Liu, S.N. Wu, Q. Wu, C.G. Quan, Y.M. Ren, A novel stereo vision measurement system using both line scan camera and frame camera, IEEE Trans. Instrum. Meas. 68 (10) (2019) 3563–3575.
[12] H.B. Duan, Q.F. Zhang, Visual measurement in simulation environment for vision-based UAV autonomous aerial refueling, IEEE Trans. Instrum. Meas. 64 (9) (2015) 2468–2480.
[13] Z.T. Zhang, D. Xu, M. Tan, Visual measurement and prediction of ball trajectory for table tennis robot, IEEE Trans. Instrum. Meas. 59 (12) (2010) 3195–3205.
[14] Y. Yang, Y. Que, S.Y. Huang, P. Lin, Multiple visual features measurement with gradient domain guided filtering for multisensor image fusion, IEEE Trans. Instrum. Meas. 66 (4) (2017) 691–703.
[15] T. Qin, P.L. Li, S.J. Shen, VINS-Mono: a robust and versatile monocular visual-inertial state estimator, IEEE Trans. Robot. 34 (4) (2018) 1004–1020.
[16] C.M. Song, X.H. Wang, B.C. Yin, D.K. Liu, Fast hierarchical wavelet-domain motion estimation for arbitrarily shaped visual objects, Inform. Sci. 55 (2019) 233–251.
[17] E.H. Lu, J. Liu, Y. Xiong, H.J. Qiu, The influences of light source and roughness ranges on colour image-based visual roughness measurement performance, Measurement 147 (2019), 106855.
[18] X.Y. Chen, J.Z. Yu, S.H. Kong, Z.X. Wu, X. Fang, L. Wen, Towards real-time advancement of underwater visual quality with GAN, IEEE Trans. Ind. Electron. 66 (12) (2019) 9350–9359.
[19] L.Z. Zhang, D.M. Wu, Y.Q. Ren, Pose measurement for non-cooperative target based on visual information, IEEE Access 7 (2019) 106179–106194.
[20] H.P. Zhang, Z.G. Jiang, A. Elgammal, Vision-based pose estimation for cooperative space objects, Acta Astronaut. 91 (10-11) (2013) 115–122.
[21] H. Pan, J.Y. Huang, S.Y. Qin, High accurate estimation of relative pose of cooperative space targets based on measurement of monocular vision imaging, Optik 125 (13) (2014) 3127–3133.
[22] S.Y. Sun, Y.J. Yin, X.G. Wang, D. Xu, Robust landmark detection and position measurement based on monocular vision for autonomous aerial refueling of UAVs, IEEE Trans. Cybernetics 49 (12) (2019) 4167–4179.

[23] S. Panev, F. Vicente, F. De la Torre, V. Prinet, Road curb detection and localization with monocular forward-view vehicle camera, IEEE Trans. Intell. Transp. 20 (9) (2019) 3568–3584.
[24] Y.Z. Zhang, W.H. Wang, P.F. Huang, Z.N. Jiang, Monocular vision-based sense and avoid of UAV using nonlinear model predictive control, Robotica 37 (9) (2019) 1582–1594.
[25] S.B. Wang, Y. Xu, Y.H. Zheng, M.C. Zhu, H.D. Yao, Z.Y. Xiao, Tracking a golf ball with high-speed stereo vision system, IEEE Trans. Instrum. Meas. 68 (8) (2019) 2742–2754.
[26] D.L. Zhao, F.F. Kong, F.Z. Du, Vision-based adaptive stereo measurement of pins on multi-type electrical connectors, Meas. Sci. Technol. 30 (10) (2019), 105002.
[27] J. Lwowski, A. Majumdar, P. Benavidez, J.J. Prevost, M. Jamshidi, Bird flocking inspired formation control for unmanned aerial vehicles using stereo camera, IEEE Syst. J. 13 (3) (2019) 3580–3589.
[28] Z. Gong, Z. Liu, G.J. Zhang, Flexible global calibration of multiple cameras with nonoverlapping fields of view using circular targets, Appl. Optics 56 (11) (2017) 3122–3131.
[29] N. Murmu, B. Chakraborty, D. Nandi, Relative velocity measurement using low cost single camera-based stereo vision system, Measurement 141 (2019) 1–11.
[30] J. Huo, N. Yang, M. Yang, J.S. Cui, Flexible calibration of camera with large FOV based on planar homography, Optik 126 (2015) 5218–5223.